Thiophene Based Metallomacrocyclic Dithiocarbamate Complexes: Synthesis, Characterization and Their Involvement in Heavy Metal Ion Sensing Study

Abstract

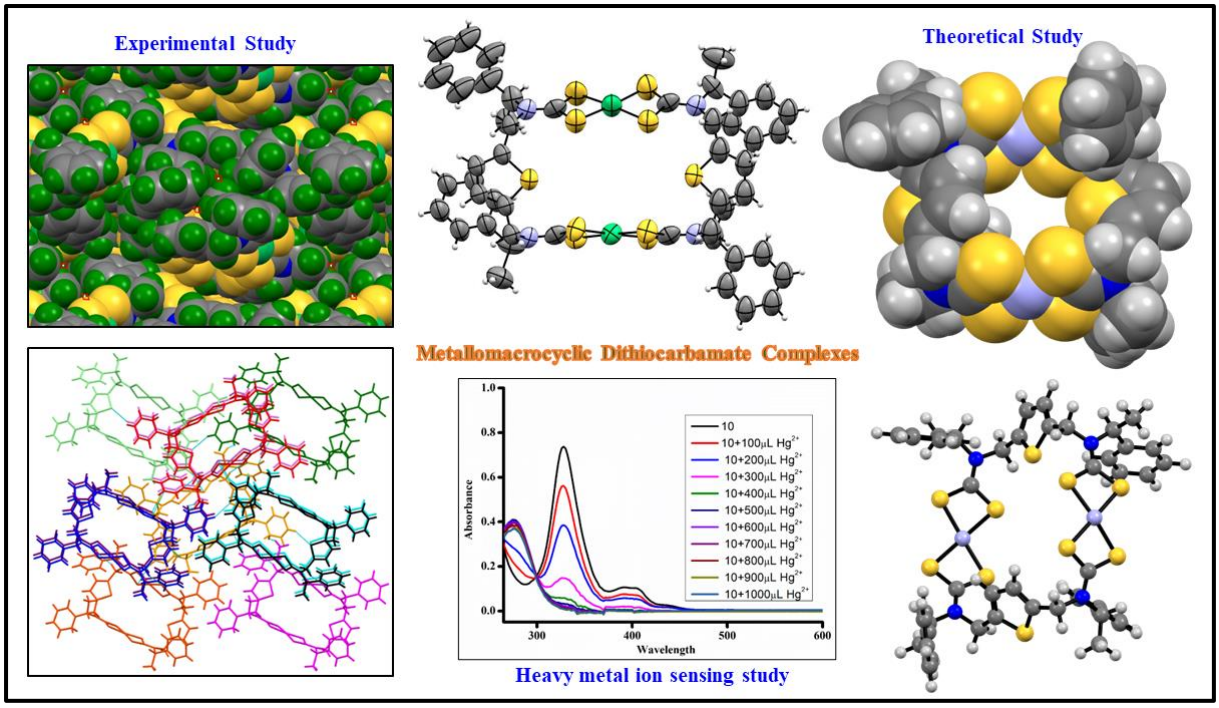

In this chapter, the secondary diamino precursors viz. *S,S*-(Thiophene-2,5-diyl)bis(N-(1-phenylethyl)methanamine) **H_2L^3** and *R,R*-(Thiophene-2,5-diyl)bis(N-(1-phenylethyl)methanamine) **H_2L^4** holding thiophene spacers prepared in chapter 2 have been successfully utilized to derive a new series of binuclear metallomacrocyclic dithiocarbamate complexes [M(II)$_2$-μ^2-bis-{(κ^2*S,S*-S_2CN(CH(*S*-CH_3)Ph)CH_2)$_2$thiophene}]; M = Ni(II) **7**, Cu(II) **8**, Zn(II) **9** and [M(II)$_2$-μ^2-bis-{(κ^2*S,S*-S_2CN(CH(*R*-CH_3)Ph)CH_2)$_2$thiophene}]; M = Ni(II) **10**, Cu(II) **11**, Zn(II) **12**. The formation and purity of all the binuclear metallomacrocyclic dithiocarbamate complexes were verified by microanalysis and standard spectroscopic methods such as HRMS, NMR, IR and UV-visible absorption spectroscopy and supported by SCXRD study as well as density functional theory calculations. The experimental and theoretical calculations suggest square planar/distorted square planar environment around nickel(II)/ copper(II) and tetrahedral/distorted tetrahedral environment around zinc(II) centres in **7-12**. Notably, the calculated HOMO-LUMO gaps (1.84-2.08 eV) for Cu(II)-

dithiocarbamate **8** and **11** indicates their semiconducting nature. The potentials of these binuclear metallomacrocycles as a molecular probe for optical sensing of environmentally hazardous heavy metal ions *ca* Pb(II), Cd(II) and Hg(II) were further examined by using UV-visible.

4.1 Introduction

Metallomacrocyclic dithiocarbamate complexes containing amines have captured considerable attention among researchers due to their diverse properties, which play a crucial role in the design and synthesis of functional molecular materials.[1–7] Particularly, noteworthy are complexes that contain optically active amines, especially those based on thiophene macrocycles. These complexes exhibit distinctive optical properties, making them valuable for applications such as organic compound sensors, colorimetric sensors, or fluorescent sensors for chiral recognition.[8–12] Among their various applications, these compounds demonstrate significant catalytic activity in diverse organic reactions.[13,14] Additionally, amines and their complexes showcase notable biological properties, including anticancer and antibacterial activities.[15,16]

The incorporation of numerous donor atoms such as O, N, S, P and the ability for supramolecular construction provide ample coordination space, leading to the formation of mono-, di-, and polynuclear complexes.[17–19] The fluorescent properties of macrocycle architecture, formed through a combination of thiophene and piperazine groups, can be notably influenced. Thiophene units, willing to functionalization at the third and fourth positions, often incorporate chiral alkyl substituents, thereby enhancing their potential.[20] By altering the number of donor atoms, diverse types of complexes can be attained. In a recent study by E. Chinnaraja et al., a one-pot synthesis was reported for a series of macrocyclic complexes [2+2]. These complexes were composed of dialdehydes, namely 4-methyl-2,6-diformylphenol or 4-tert-butyl-2,6-diformylphenol and chiral amines as building blocks, with Cu(II) metal salt employed in the synthesis.[21] The resulting compounds exhibited enantiomeric purity, displayed chiroptical properties, and demonstrated catalytic activity in various organic transformations.[22–24] The design, synthesis, and modification of such complexes have attracted significant attention, particularly for their potential impact on the field of molecular magnetism.[25,26] Investigating the magnetic interaction between central metal ions Ni^{II}, Cu^{II} and Zn^{II} in multinuclear complexes is a key focus in the study of heavy metal ion sensing.[27,28] Given these properties, the recognition of binuclear macrocyclic complexes with Ni^{II}, Cu^{II} and Zn^{II} is warranted.[29–31]

Consequently, the ongoing quest for new compounds exhibiting both fluorescent and magnetic properties, suitable for application in thin films, continues. The properties of the materials depend on the presence of substituents, their electronic nature, or the presence and size of the aromatic rings. Hence, this study presents the synthesis, structural elucidation, and examination of the magnetic and spectroscopic features of binuclear macrocyclic complexes involving Ni^{II}, Cu^{II} and Zn^{II}. These complexes were obtained through a one-pot reaction using *S, S*-(Thiophene-2,5-diyl)bis(N-(1-phenylethyl)methanamine) **H_2L^3** and *R, R*-(Thiophene-2,5-diyl)bis(N-(1-phenylethyl)-methanamine) **H_2L^4** with $Ni(OAc)_2{\cdot}4H_2O$, $Cu(OAc)_2{\cdot}H_2O$, $Zn(OAc)_2{\cdot}2H_2O$. Additionally, DFT calculations were performed to substantiate the magnetic behaviour and optical properties of the complexes. Furthermore, the novel Ni^{II}, Cu^{II} and Zn^{II} complexes were employed in a study focused on heavy metal ion sensing in DMSO solution.

In the current work, Fascinating potential applications of binuclear metallomacrocyclic dithiocarbamate complexes have encouraged us to synthesize a new series of metallomacrocyclic dithiocarbamate complexes [M(II)$_2$-μ^2-bis-{(κ^2*S,S*-S_2CN(CH(*S*-CH_3)Ph)CH_2)$_2$thiophene}]; M = Ni(II) **7**, Cu(II) **8**, Zn(II) **9** and [M(II)$_2$-μ^2-bis-{(κ^2*S,S*-S_2CN(CH(*R*-CH_3)Ph)CH_2)$_2$thiophene}]; M = Ni(II) **10**, Cu(II) **11**, Zn(II) **12**, holding thiophene linkers. The compounds **10-12** were investigated for their potential small-molecule probes in the sensing of heavy metal ions viz. Pb(II), Cd(II) and Hg(II) by using UV-visible absorption spectroscopy. The incorporation of the soft sulphur atoms and with their added features to show variable coordination number, geometry, oxidation state, color, redox, electronic, steric and magnetic properties, in combination with functionalized organic ligands, these metallomacrocyclic dithiocarbamate complexes can be established as better small-molecule probe in the sensing and recovery of heavy metal ions through effective sensitivity, selectivity and binding affinity towards Pb(II), Cd(II) and Hg(II) heavy metal ions.

4.2 Experimental Section

4.2.1 Materials and Instrumentations

All the synthetic manipulations were performed in an open atmosphere. The solvents were of laboratory grade available at various commercial sources and distilled prior to use by following the standard procedures. Potassium hydroxide (97%) (Fisher Scientific), carbon disulfide (99%) (Fisher Scientific), metal acetates such as $Ni(OAc)_2{\cdot}4H_2O$, $Cu(OAc)_2{\cdot}H_2O$, $Zn(OAc)_2{\cdot}2H_2O$ (98%) (all Merck), Ligand precursors *S,S*-(Thiophene-2,5-diyl)bis(N-(1-phenylethyl)methanamine) **H_2L^3** and *R,R*-(Thiophene-2,5-diyl)bis(N-(1-phenylethyl)-methanamine) **H_2L^4** were synthesized in Chapter 2. The reaction and manipulations were

performed at room temperature. Thin Layer Chromatography was performed on Merck 60 F254 aluminium-coated plates. Elemental analyses were performed on a Perkin-Elmer Series II CHNS Analyzer 2400. High resolution mass spectrometry (HR-MS) analysis was performed by using an instrument Waters, Synapt XS HDMS containing a separation module of UPLC Acquity H class series system under electro spray positive (ES+) ionization mode. FTIR (KBr pellets) spectra of the samples were recorded in the 4000–400 cm^{-1} range using a Bruker FTIR spectrometer. The NMR experiments were carried out on a Bruker AV-III 400 MHz spectrometer in spectrometer with $CDCl_3$ solvent and TMS as internal standard. UV-visible absorption and fluorescence spectra were recorded on a JASCO V-730 UV-visible and JASCO FP 8200 spectrophotometer, respectively. TGA/DTA plots were obtained using SII TG/DTA 6300 in flowing N_2 with a heating rate of 10 °C min^{-1}. The geometry of the molecules was optimized with the Gaussian 16 program and molecular orbitals were generated using GaussView 6.0 program.

4.2.2 Synthesis of Binuclear metallomacrocyclic dithiocarbamate complexes M(II)$_2$-μ^2-bis-{(κ^2*S*,*S*-$S_2CN(CH($*S*-$CH_3)Ph)CH_2)_2$thiophene}]; M = Ni(II) 7, Cu(II) 8, Zn(II) 9 and [M(II)$_2$-μ^2-bis-{(κ^2*S*,*S*-$S_2CN(CH($*R*-$CH_3)Ph)CH_2)_2$thiophene}]; M = Ni(II) 10, Cu(II) 11, Zn(II) 12

To a solution of 1 equivalent of diamine ligands *S*,*S*-(Thiophene-2,5-diyl)bis(N-(1-phenylethyl)methanamine) **H_2L^3** (0.35 g, 1 mmol) or *R*,*R*-(Thiophene-2,5-diyl)bis(N-(1-phenylethyl)methanamine) **H_2L^4** (0.35 g, 1 mmol) in acetonitrile, 2.1 equivalent potassium hydroxide (0.12 g, 2.1 mmol) was added and the reaction mixture was stirred for half an hour at room temperature. An excess of carbon disulphide (~10 mmol) was then added and the reaction mixture was continued to stirred for further 8 hours at room temperature. During this time period, a change in colour from pale yellow to yellow was observed. To this reaction mixture, $Ni^{II}(C_2H_3O_2)_2.4H_2O$ (0.27 g, 1.1 mmol), $Cu^{II}(C_2H_3O_2)_2.H_2O$ (0.22 g, 1.1 mmol) or $Zn^{II}(C_2H_3O_2)_2.2H_2O$ (0.24 g, 1.1 mmol) was added and the stirring was continued for another 12 hours. The residue was filtered and washed several times by water followed by n-hexane. The residue was dried under high vacuum to yield the corresponding binuclear metallomacrocyclic dithiocarbamate complexes **7-12**. The compounds are taken for experimental study.

Table 1. Micro- and IR analysis data for complexes **7-12**.

Entry	Molecular Formula	Molecular Weight	Yield (%)	Melting/Dec. Point (°C)	Elemental Analysis % Found (calculated)				IR data (KBr disc) υ_{max}/cm^{-1}
					C	H	N	S	
7	$C_{48}H_{48}N_4Ni_2S_{10}$	1118.93	70	292	51.57 (51.53)	4.36 (4.32)	5.06 (5.01)	28.69 (28.65)	3419(w), 3058(w), 3026(w), 2971(w), 2924(w), 1455(vs), 1419(m), 1331(m), 1255(w), 1203(w), 1174(w), 1127(m), 1069(w), 1045(w), 996(w), 944(w), 782(w), 753(w), 697(m), 619(w), 576(w), 521(w)
8	$C_{48}H_{48}Cu_2N_4S_{10}$	1128.63	68	212	51.13 (51.08)	4.34 (4.29)	4.99 (4.96)	28.46 (28.41)	3428(w), 3057(w), 3027(w), 2973(w), 2929(w), 1450(vs), 1414(m), 1328(m), 1254(w), 1205(w), 1127(w), 1041(w), 997(w), 948(w), 781(w), 697(m), 658(w), 574(w), 521(w)
9	$C_{48}H_{48}N_4S_{10}Zn_2$	1132.30	57	268	50.98 (50.92)	4.33 (4.27)	4.99 (4.95)	28.35 (28.31)	3413(w), 3058(w), 3027(w), 2974(w), 2929(w), 1575(w), 1490(w), 1446(s), 1408(m), 1370(w), 1323(m), 1256(w), 1206(w), 1124(m), 1068(w), 1027(w), 998(w), 945(w), 782(w), 743(w), 697(m), 618(w), 568(w), 519(w)
10	$C_{48}H_{48}N_4Ni_2S_{10}$	1118.93	72	290	51.57 (51.53)	4.33 (4.32)	5.07 (5.01)	28.69 (28.65)	3423(w), 3058(w), 3027(w), 2972(w), 2928(w), 1485(w), 1454(s), 1418(m), 1333(w), 1253(w), 1204(w), 1175(w), 1127(w), 1045(m), 997(w), 943(w), 782(w), 749(w), 696(w), 576(w), 517(w)
11	$C_{48}H_{48}Cu_2N_4S_{10}$	1128.63	66	202	51.12 (51.08)	4.35 (4.29)	5.01 (4.96)	28.46 (28.41)	3424(w), 3058(w), 3027(w), 2972(w), 2928(w), 1670(w), 1448(s), 1413(m), 1327(w), 1252(w), 1206(w), 1125(w), 1045(w), 996(w), 943(w), 782(w), 749(w), 697(w), 570(w), 519(w).
12	$C_{48}H_{48}N_4S_{10}Zn_2$	1132.30	54	254	50.97 (50.92)	4.33 (4.27)	4.99 (4.95)	28.35 (28.31)	3423(w), 3057(w), 3027(w), 2972(w), 2929(w), 1492(w), 1448(s), 1406(w), 1371(w), 1323(w), 1259(w), 1203(w), 1154(w), 1124(w), 1068(w), 1045(w), 1026(w), 999(w), 946(w), 783(w), 760(w), 697(m), 616(w), 568(w), 525(w)

Table 2. NMR spectral data for complexes **7, 9, 10** and **12**.

Entry	NMR Data (ppm)	
	^{1}H NMR	**^{13}C NMR**
7	7.28–7.45 (m, 20 H, Ph); 6.10-6.57 (s, 4H, -thiophene); 4.84 (s, 8H, -CH_2); 4.28-4.32 (m, 4H, -CH); 1.54 (d, 12H, -CH_3)	209.32(-*NCS_2*), 137.16, 128.60, 128.23, 128.11, 127.96, 125.92, 56.51, 44.21, 16.37
9	7.28–7.41 (m, 20 H, Ph); 6.59-6.72 (s, 4H, -thiophene); 4.60 (s, 8H, -CH_2); 3.81-3.88 (m, 4H, -CH); 1.57 (d, 12H, -CH_3)	206.0 (-*NCS_2*), 138.2 ,136.7, 128.9, 128.8, 128.6, 128.3, 127.7, 127.2, 127.0, 126.8, 126.6, 126.1, 62.5, 57.0, 48.2, 45.8, 23.8, 16.6
10	7.28–7.45 (m, 20 H, Ph); 6.10-6.57 (s, 4H, -thiophene); 4.83 (s, 8H, -CH_2); 4.31 (m, 4H, -CH); 1.38-1.54 (d, 12H, -CH_3)	-
12	7.28–7.38 (m, 20 H, Ph); 6.58-6.63 (s, 4H, -thiophene); 4.59 (s, 8H, -CH_2); 4.48 (m, 4H, -CH); 1.28-1.66 (d, 12H, -CH_3)	-

4.3 Result and Discussion

4.3.1 Synthesis and Characterization

As we discussed in chapter 2, secondary diamines containing thiophene linkers, specifically *S*,*S*-(Thiophene-2,5-diyl)bis(N-(1-phenylethyl)methanamine) (**H_2L^3**) and *R*,*R*-(Thiophene-2,5-diyl)bis(N-(1-phenylethyl)methanamine) (**H_2L^4**) have been synthesized and characterized before being used in the synthesis of a new series of binuclear metallomacrocyclic dithiocarbamate complexes [M(II)$_2$-μ^2-bis-{(κ^2*S*,*S*-$S_2CN(CH(S\text{-}CH_3)Ph)CH_2)_2$thiophene}]; M = Ni(II) **7**, Cu(II) **8**, Zn(II) **9** and [M(II)$_2$-μ^2-bis-{(κ^2*S*,*S*-$S_2CN(CH(R\text{-}CH_3)Ph)CH_2)_2$thiophene}]; M = Ni(II) **10**, Cu(II) **11**, Zn(II) **12**, holding thiophene linkers (Scheme 1). These sulfur-rich metallomacrocycles are synthesized using a one-pot reaction methodology, which has abundant unique advantages. It includes multiple chemical reactions in one vessel at once, shortens the workup, and ultimately saves valuable resources.

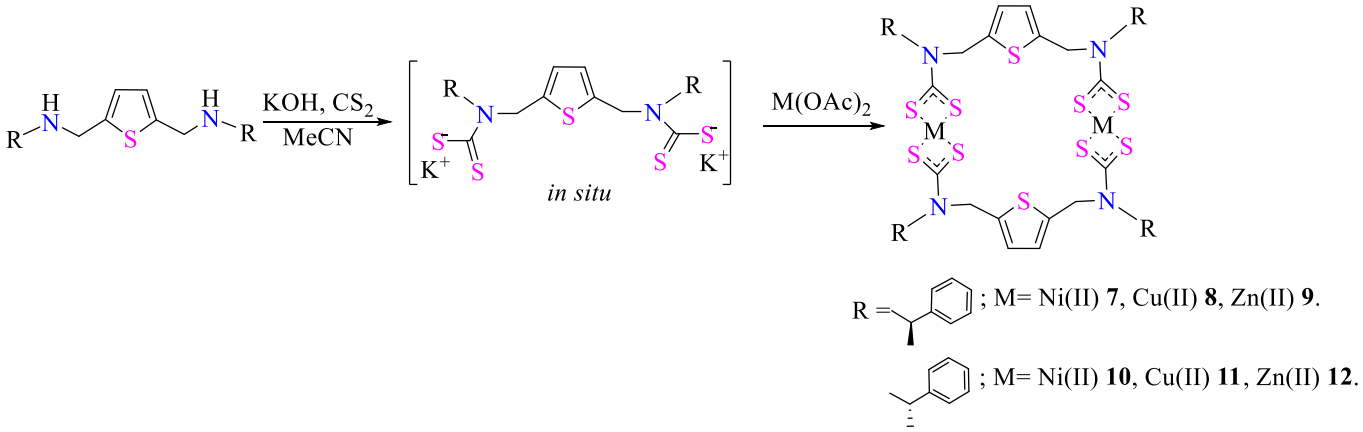

Scheme 1. One-pot multi-component synthetic protocol used for binuclear $Ni^{II}/Cu^{II}/Zn^{II}$ dithiocarbamate metallomacrocyclic compounds holding thiophene in linker framework.

The green coloured Ni(II)-dithiocarbamate compounds (**7, 10**), brown coloured Cu(II)-dithiocarbamate compounds (**8, 11**), and pale yellow coloured Zn(II)-dithiocarbamate compounds (**9, 12**) showed good solubility in $CHCl_3$, acetone, DMF, DMSO. The products appeared to be stable in the solid form and in the solution state for days.

The compounds were characterized by microanalysis, HRMS (High resolution mass spectrometry), thermogravimetric analysis and relevant spectroscopic techniques. As shown in table 1 and table 2, the microanalysis and spectroscopic data were sufficient to unequivocally assign the structure of metallomacrocyclic dithiocarbamate complexes **7-12** which were further corroborated by DFT study. The mass analysis was carried out by electrospray ionization (ESI) mode with set parameters, such as gas temperature: 250 °C; drying gas flow: 12 $Lmin^{-1}$; nebulizer

pressure: 35 psig; sheath gas flow: 11 $Lmin^{-1}$, sheath gas temperature: 300 °C. The scan source parameters were maintained at capillary voltage: 3.5KV; nozzle voltage: 1.0KV, fragmentor voltage: 175 V; skimmer voltage: 65 V. Mass spectrometric data was processed using MassHunter™ B.08.00 software. HRMS spectra of compounds **7**, **8** and **9** (Annexure **1-3**) gave high resolution mass peak for **7 (**$C_{48}H_{48}N_4Ni_2S_{10}$), **8 (**$C_{48}H_{48}Cu_2N_4S_{10}$) and **9 (**$C_{48}H_{48}N_4S_{10}Zn_2$) are observed at 1116.6180 $[M+H]^+$, 1126.9757 $[M+H]^+$ and 1128.9822 $[M+H]^+$ respectively.

All the compounds displayed characteristic IR bands due to ν(C=C), ν(C-N), ν(C-C) and ν(CS_2) in the expected IR regions. Notably, A new single sharp medium intensity band at ~998 cm^{-1} due to $\nu_{assy}(CS_2)$ stretching vibrations in the IR spectra of ensuing metallomacrocyclic compounds **7-12** offered primary indication of bidentate coordination of dithiocarbamate ligands. Besides, the ν(M-S) bands which depends on the metal ion and the auxiliary ligands, appears as weak intensity bands in 517-525 cm^{-1} range.[32] The IR data is well supported by corresponding NMR spectral study. The presence of benzylic, chiral CH, methyl and methylene groups in the molecules are conformed by ^1H and ^{13}C NMR data as shown in table 2. Remarkably, the downfield shifting of *N*-methylene signals by ~1 ppm, compared to their positions in free diamines, further supports the formation metallomacrocyclic compounds **7-12** as these signals are most sensitive to any kind of chemical change at amino group. The binuclear metallomacrocyclic dithiocarbamate macrocyclic complexes show a very downfield ^{13}C NMR signal in δ 209.3-206.0 ppm range, characteristic of coordinated dithiocarbamate *(-$N^{13}CS_2$)* moiety.

4.3.2 UV-Visible absorption spectral study

The electronic absorption spectrum of metallomacrocyclic dithiocarbamate complexes **7-12** was recorded in 10^{-5} M $CHCl_3$ solution at room temperature (Figure 1, Table 4) and the UV-visible absorption spectral study revealed that Ni(II)-dithiocarbamate complexes **7** and **10** primarily absorbs at ~255 nm, ~320 nm, ~400 nm and ~635 nm attributable to π→π* (phenyl), n→π*, charge transfer and d-d transitions, respectively, whereas, that Cu(II)-dithiocarbamate complexes **8** and **11** primarily absorbs at ~260 nm, ~295 nm, ~438 nm and ~650 nm attributable to π→π* (phenyl), n→π*, charge transfer and d-d transitions, respectively. Zn(II)-dithiocarbamate complexes **9** and **12** exhibited featureless absorption spectra presenting a broad absorption at ~260 nm due to intra-ligand π→π* transitions.

Magnetic moment along with UV-visible absorption bands indicate that the environments surrounding the centre of nickel(II)/copper(II) complexes are square planar/distorted square planar and environment around centre of zinc(II) complexes are tetrahedral/distorted tetrahedral in their respective complexes.

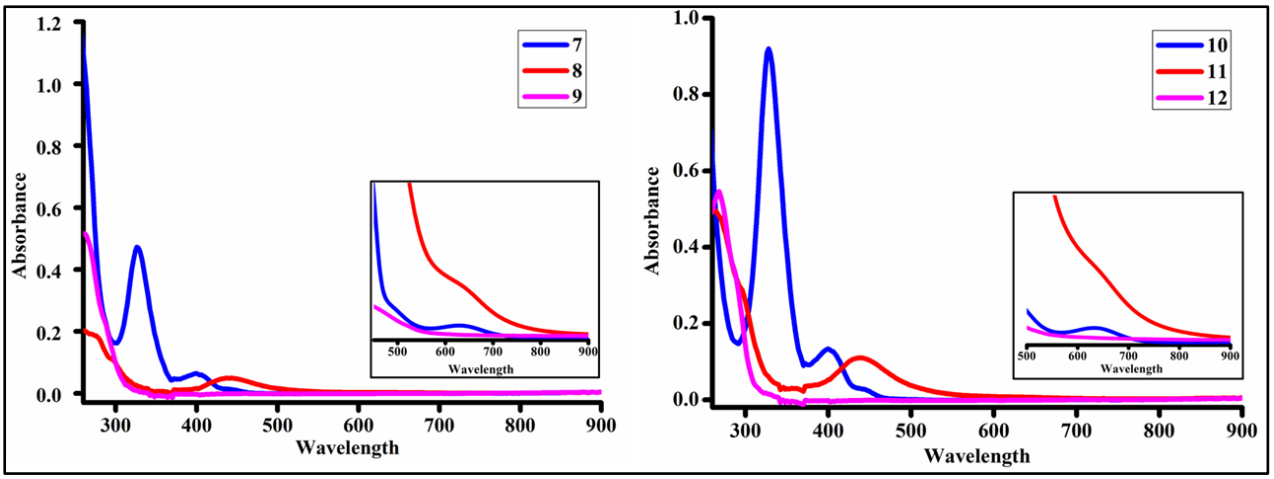

Figure 1. UV-visible absorption spectra of metallomacrocyclic dithiocarbamate complexes **7-12** in 10^{-5} M $CHCl_3$ solution at room temperature.

Table 3. UV-visible absorption and magnetic moment data for metallomacrocyclic dithiocarbamate complexes **7-12**.

Entry	UV-Visible data (10^{-5} M $CHCl_3$) λ_{max} nm (ε, L mol^{-1} cm^{-1})	Magnetic moment μ_{eff} (BM)
7	258 (112297) π→π*, 326 (47774) n→π*, 399 (6484) CT, 637(1617) d-d	0
8	258 (20348) π→π*, 297 (10822) n→π*, 438 (5154) CT, 641(657) d-d	1.85
9	261 (51819) π→π*	0
10	251 (93851) π→π*, 327 (92272) n→π*, 400 (13406) CT, 634 (2114) d-d	0
11	263 (49499) π→π*, 296 (28851) n→π*, 438 (11048) CT, 647 (938) d-d	1.82
12	267 (54659) π→π*	0

4.3.3 X-ray Crystallographic Study

The single crystals of complex **7** and **10** suitable for single crystal X-ray diffraction (SCXRD) study were grown by slow evaporation from dichloromethane and acetone solution, respectively. Both the complexes **7** and **10** are crystallized in the orthorhombic $P2_12_12_1$ space group. The X-ray crystal structures of **7** and **10** are shown in Figure 2. The crystallographic data and structure parameters for **7** and **10** are given in Table 4.

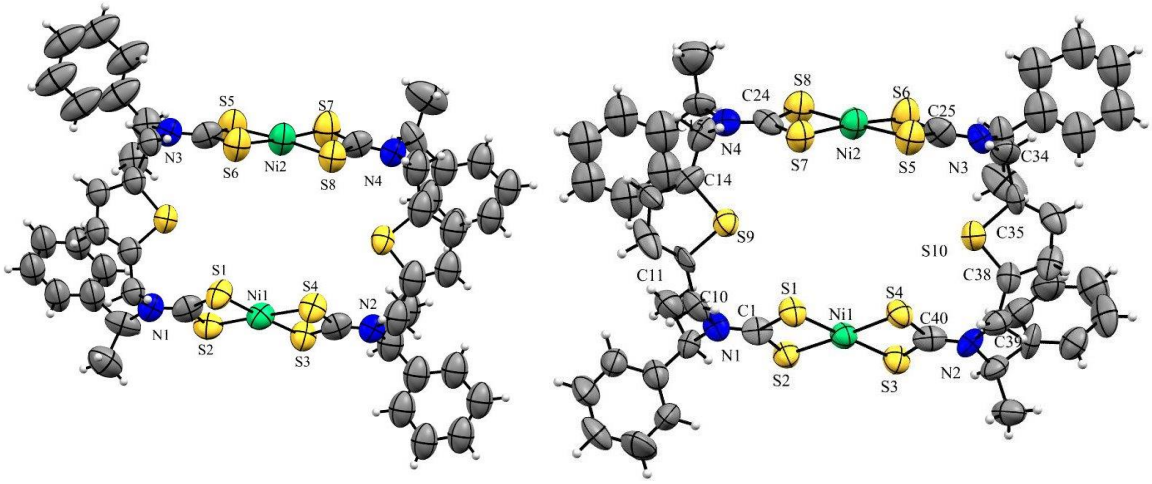

Complex **7** Complex **10**

Figure 2. X-ray structure of complex **7** and **10** with atom numbering scheme.

Table 4. Crystal data and structure parameters for the complexes **7** and **10**.

Identification code	**7**	**10.$(CH_3)_2CO$**
Empirical formula	$C_{48}H_{50}N_4Ni_2S_{10}$	$C_{51}H_{55}N_4Ni_2OS_{10}$
Formula weight	1120.94	1178.01
Temperature/K	293(2)	293
Crystal system	orthorhombic	orthorhombic
Space group	$P2_12_12_1$	$P2_12_12_1$
a/Å	14.045(3)	14.131(2)
b/Å	18.679(3)	18.5745(15)
c/Å	21.648(3)	21.789(2)
α/°	90.00	90.00
β/°	90.00	90.00
γ/°	90.00	90.00
Volume/$Å^3$	5679.1(16)	5719.1(11)
Z	4	4
$\rho_{calc}g/cm^3$	1.311	1.368
μ/mm^{-1}	1.065	1.063
F(000)	2328.0	2452.0
Crystal size/mm^3	0.2 × 0.1 × 0.05	0.25 × 0.2 × 0.1
Radiation	Mo Kα (λ = 0.71073)	Mo Kα (λ = 0.71073)
2Θ range for data collection/°	6.06 to 44.8	6.06 to 50.8°
Index ranges	$-15 \le h \le 15$, $-19 \le k \le 20$, $-23 \le l \le 23$	$-15 \le h \le 15$, $-19 \le k \le 19$, $-23 \le l \le 23$
Reflections collected	22553	22658
Independent reflections	7294 [R_{int} = 0.2399, R_{sigma} = 0.3013]	7356[R(int) = 0.1315]
Data/restraints/parameters	7294/3/335	7356/0/553
Goodness-of-fit on F^2	0.995	1.202

Final R indexes [I>=2σ (I)]	R_1 = 0.1212, wR_2 = 0.2240	R_1 = 0.1085, wR_2 = 0.2289
Final R indexes [all data]	R_1 = 0.2996, wR_2 = 0.3138	R_1 = 0.1828, wR_2 = 0.2794
Largest diff. peak/hole / e $Å^{-3}$	0.65/-0.34	0.86/-0.42
Flack parameter	-0.05(6)	-0.01(4)

The molecule presents in the asymmetric unit of complex **7** holding *S*-chirality evidently offers a vast number of intermolecular CH…S, $\pi_{aromatic}$…$\pi_{chelate}$ and CH…pi contacts and forms a supramolecular aggregate consisting of 11 molecules. The overall supramolecular assembly sustained by these interaction displays good number of 3D pores of dimension 5 × 18 $Å^2$ in the soiled state which may fall under the microporous materials (Figure 3).

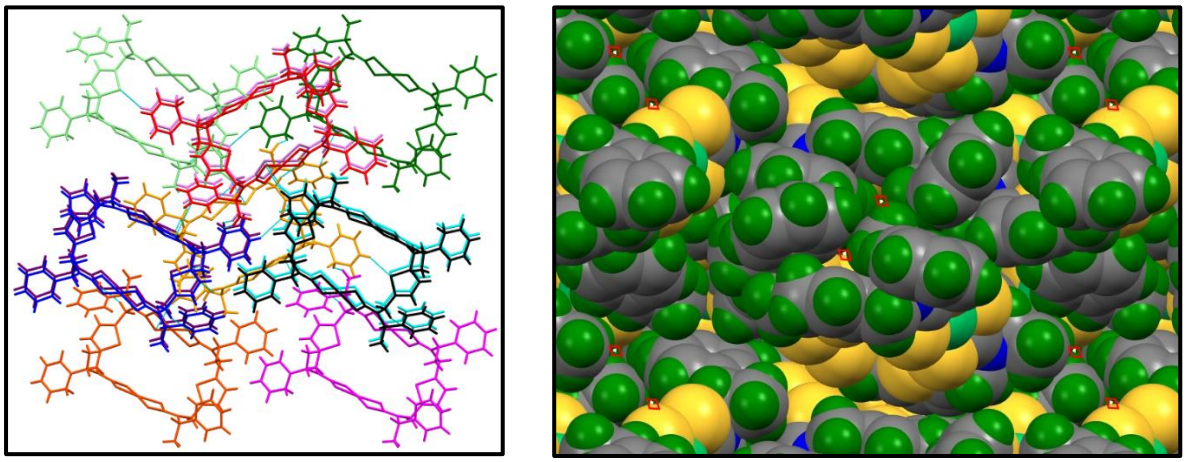

(a) **(b)**

Figure 3. (a) Each molecule of complex 7 offer intermolecular CH…S, $\pi_{aromatic}$… $\pi_{chelate}$ and CH…pi contacts **(b)** Supramolecular assembly of complex **7** displays 3D pores of dimension 5 × 18 $Å^2$ which may fall under the microporous materials

Complex **10** crystallizes in the form of **10**.$(CH_3)_2CO$ and the molecule present in the asymmetric unit holding *R*-chirality offers a good number of intermolecular CH….O and CH….S contacts and forms a supramolecular aggregate consists of 7 molecules which is shown in Figure 4. Interestingly, the introduction of *R*-chirality at benzylic carbon diminished the CH…pi contacts seen in the crystal packing of complex **7** holding *S*-chirality and supports the involvement of acetone solvent in the formation of several CH…O intermolecular contacts.

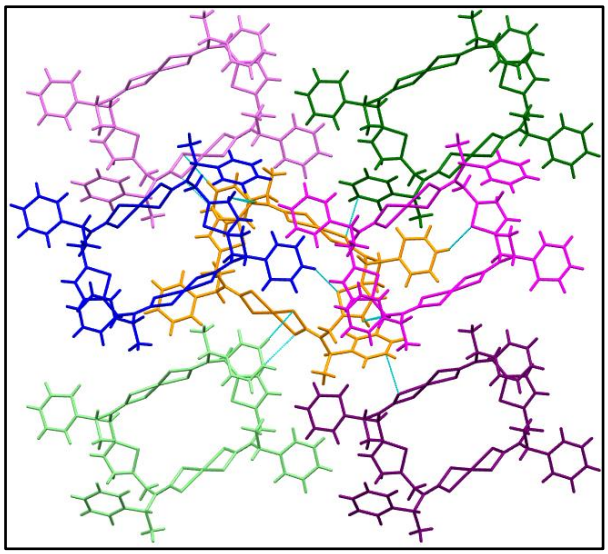

Figure 4. Each molecule of complex **10** offer intermolecular CH…O and CH…S contacts

4.3.4 Thermogravimetric Analysis

The thermogravimetric analysis was performed on the binuclear metallomacrocyclic dithiocarbamate complexes **7-12** up to 500 ºC. The heating rate was appropriately regulated at 10 ºC min^{-1} in an atmosphere of nitrogen. The DTG curves of complexes **7-12** clearly show their diverse rate of degradation, and they are thermally stable up to ~220 ºC. (Table 5) The TG curves of compounds **10** and **12** gave the mass loss of 71.3 and 68.2 % respectively, and thus their stable residual mass obtained at 500 ºC corresponds to corresponding metal sulphate, whereas, the TG curves of compounds **7, 8, 9** and **11** gave the mass loss of 65.7, 62.4, 63.4 and 63.4 % respectively, so, their stable residual mass obtained at 500 ºC corresponds to corresponding metal sulphate including some amount of char.

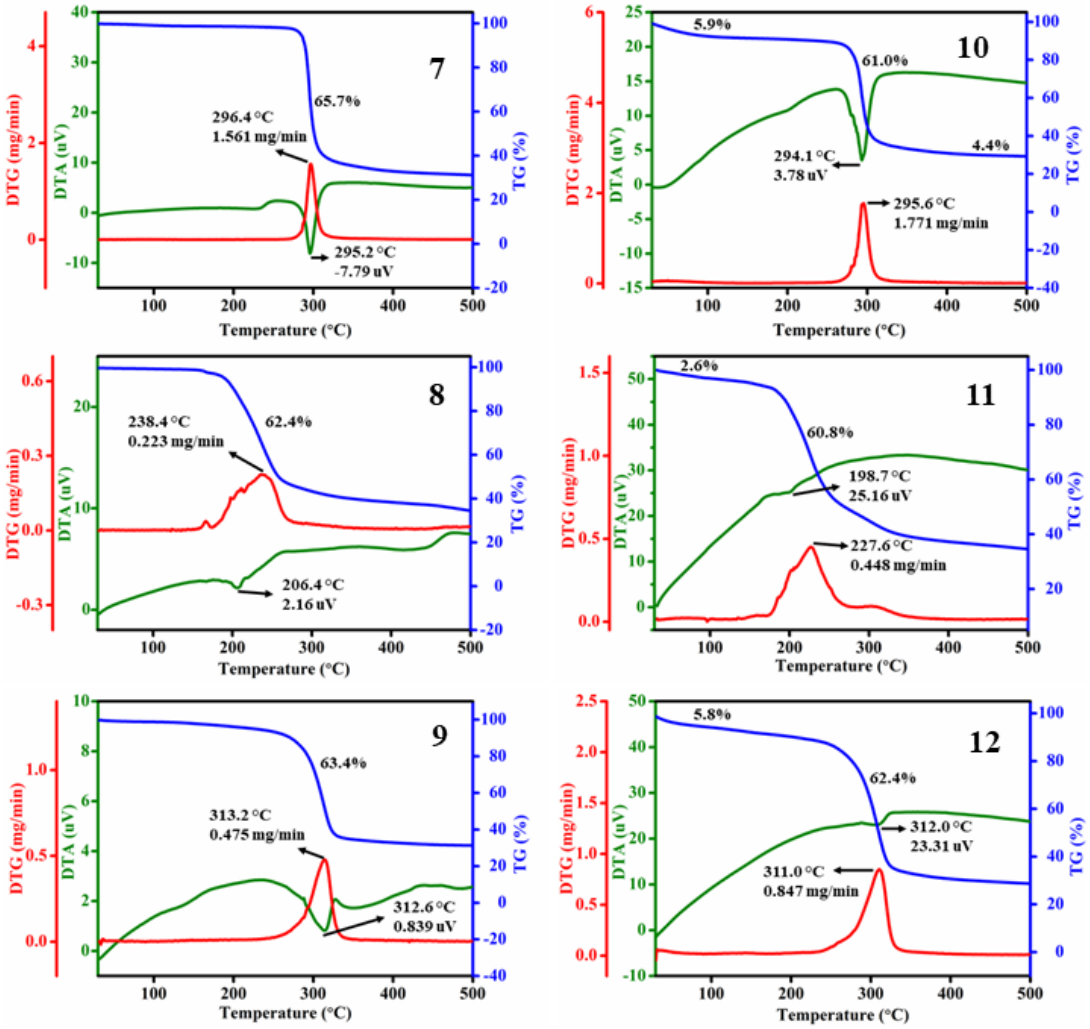

Figure 5. TG/DTA curves for metallomacrocyclic dithiocarbamate complexes **7-12**.

Table 5. Thermogravimetric analysis of metallomacrocyclic dithiocarbamate complexes **7-12.**

Entry	T (°C) in DTA	T (°C) in TGA	Mass loss obs. (%) in TG	Residue wt. obs. (Calcd.) (%)	Expected product of decomposition
7	295.2	280-400	65.7	34.3 (27.6)	$NiSO_4$ + char
8	206.4	175-400	62.4	37.6 (28.3)	$CuSO_4$ + char
9	312.6	250-400	63.4	36.6 (28.5)	$ZnSO_4$ + char
10	-	50-150	5.9	28.7 (27.6)	$NiSO_4$
	294.1	150-400	61.0		
	-	400-500	4.4		
11	-	40-110	2.6	36.6 (28.3)	$CuSO_4$ + char
	198.7	110-400	60.8		
12	-	40-150	5.8	31.8 (28.5)	$ZnSO_4$
	312.0	150-420	62.4		

4.3.5 Density functional theory calculations

Density functional theory level calculations and full geometry optimizations were carried out for binuclear dithiocarbamate complexes **7-12** using B3LYP/LanL2DZ basis sets and the molecular orbitals were generated by GaussView 16.0 program The optimized structures for the minimum energy conformation of complexes **7-12** are presented in Figure 6.

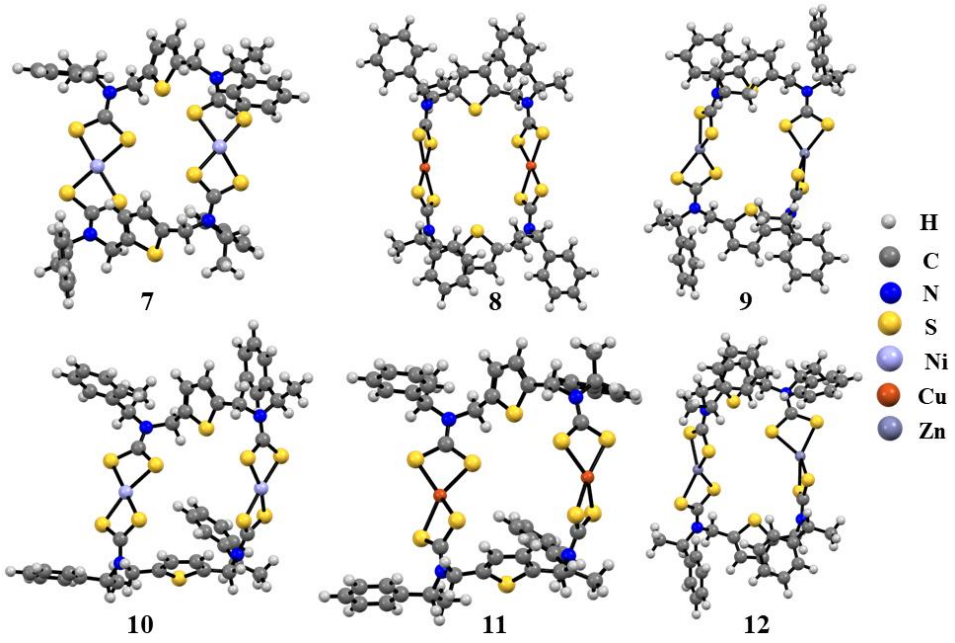

Figure 6. An optimized geometry for the minimum energy conformation of complexes **7-12** at B3LYP/LanL2DZ level.

The structural parameters (selected bond lengths and bond angles) of binuclear metallomacrocyclic dithiocarbamate complexes **7-12** (Table 6) are found to be consistent with the similar parameters deduced experimentally for analogous compounds[33a,33b] by means of single crystal XRD.

Table 6. Comparison of selected geometrical parameters for macrocyclic dithiocarbamate complexes **7-12** obtained from theoretical study with similar experimental parameters.

Entry	**Bond length (Å)**						**Bond angles (°)**	
	N-C	C-S	M-S	Trans-annular M-M	S-S (Thiophene)	N-N (trans NCS_2)	S-M-S (chelate)	S-M-S
7	1.344 to 1.346	1.725 to 1.737	2.272 to 2.282	8.209	9.190	10.268 to 10.981	78.14 to 78.23	168.67 to 177.96
7 (present work)	1.263 to 1.357	1.687 to 1.752	2.192 to 2.224	6.352	7.801	10.067 to 10.249	79.16 to 80.29	174.06 to 178.13
10	1.345 to 1.349	1.725 to 1.736	2.257 to 2.296	7.709	8.541	8.948 to 11.371	78.08 to 78.16	163.23 to 175.90
10 (present work)	1.266 to 1.323	1.700 to 1.762	2.196 to 2.229	6.669	7.771	10.171 to 10.309	79.13 to 79.71	173.70 to 178.26

8	1.344	1.734 to 1.739	2.394 to 2.400	6.936	8.069	10.478 to 10.742	75.21 to 75.24	175.36 to 178.36
11	1.346 to 1.350	1.730 to 1.740	2.379 to 2.404	7.773	8.887	9.646 to 11.203	75.19 to 75.41	149.33 to 168.22
Cu^{II}-dtc[33a]	1.318 to 1.328	1.719 to 1.727	2.288 to 2.301	-	-	-	77.59	101.72 to 103.48
9	1.345 to 1.346	1.739 to 1.754	2.441 to 2.452	6.926	7.914	9.326 to 10.677	75.35 to 75.64	132.65 to 141.46
12	1.345 to 1.348	1.741 to 1.752	2.441 to 2.457	7.063	7.928	9.805 to 10.357	75.12 to 75.38	119.80 to 140.82
Zn^{II}-dtc[33b]	1.333 to 1.363	1.717 to 1.782	2.32 to 2.44	-	-	-	79.5 to 81.2	126.53 to 136.00

The macrocyclic cavities in these compounds clearly visible in the macrocyclic framework. A virtual view of the molecular structures corresponding to the calculated lowest-energy structures of the binuclear dithiocarbamate complexes **7-12** is displayed in Figure 7.

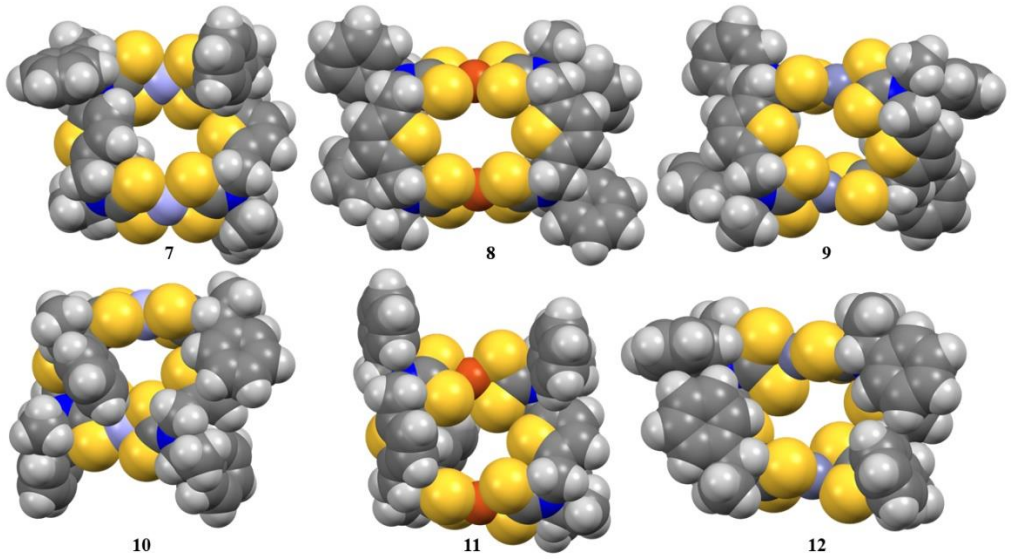

Figure 7. Spacefill model of the macrocyclic cavity in **7-12**.

The molecular electrostatic potentials of **7-12** were determined theoretically, suggesting localisation of negative potential around chelate rings and positive potentials around C-H groups (Figure 8) and confirms the ability of these molecules to offer donor-acceptors intermolecular contacts in the solid state which is indeed verified experimentally by single crystal X-ray diffraction study.

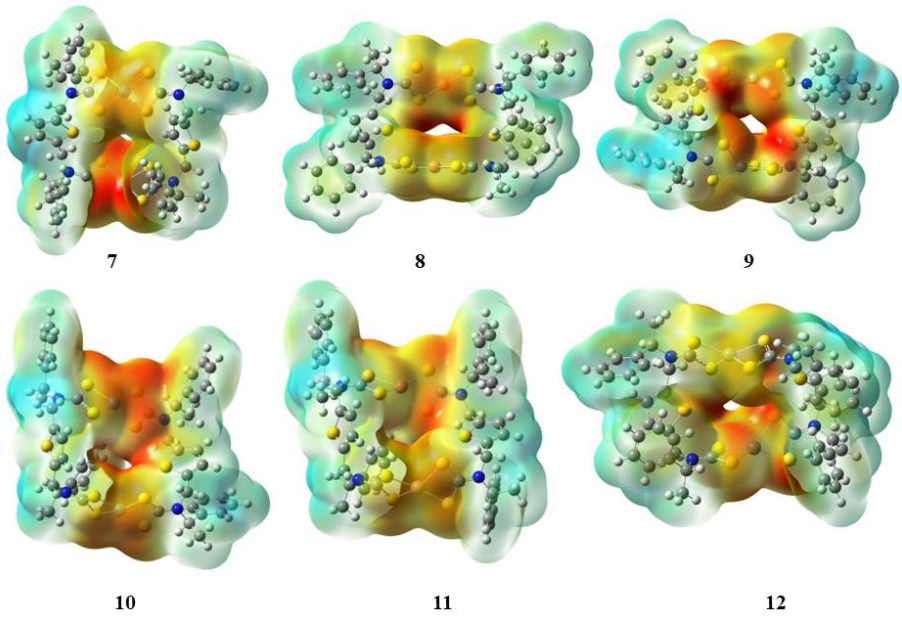

Figure 8. Representations of electron density from total SCF density (Isovalue= 0.0004; mapped with ESP)

The calculated HOMO-LUMO energy gaps for binuclear metallomacrocyclic dithiocarbamate complexes **7-12** are given in Table 7 is illustrated in Figure 9. Notably, the HOMO-LUMO band gaps calculated for both the Cu(II)-dithiocarbamate (**8, 11**) falls in the range of 1.84-2.08 eV, indicating their semiconducting nature.[34]

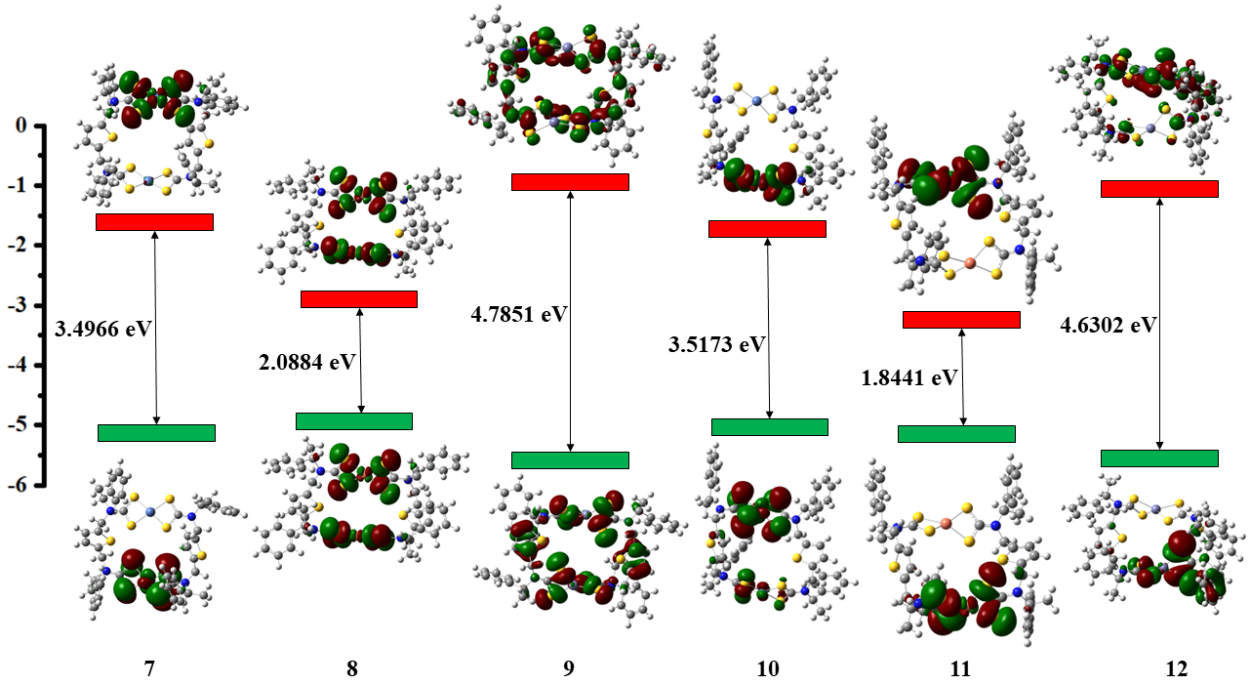

Figure 9. Comparison of the frontier molecular orbitals derived from DFT calculation at the B3LYP/ LanL2DZ level for metallomacrocyclic dithiocarbamate complexes **7-12.**

The energy of geometry optimization and HOMO-LUMO band gaps for binuclear metallomacrocyclic dithiocarbamate complexes **7-12** are presented in Table 7.

Table 7. Summary of Computational study performed on complexes **13-18.**

Entry	Energy (Hartree)	HOMO (eV)	LUMO (eV)	Band Gap (eV)
7	-6397.645641	-5.3522	-1.8664	3.4966
8	-6457.325315	-5.1269	-3.3045	2.0884
9	-6190.231424	-5.8219	-1.0827	4.7851
10	-6397.622662	-5.3838	-1.8555	3.5173
11	-6451.281881	-5.1487	-3.0384	1.8441
12	-6190.208766	-5.7130	-1.0367	4.6302

4.4 Heavy metal ions sensing study

It is believd that macrocyclic dithiocarbamate compounds **7–12** holding Lewis basic coordinating groups would be promising molecular probe for recognizing and binding of toxic metal ions such as Pb(II), Cd(II), and Hg(II). Investigations on new probe that is cost effective, rapid, facile and applicable to the environmental settings is an important goal of sensing societies due to current concern over heavy metal ions in the environment and its toxic effects on human health. In the light of lack of optical sign of Pb(II), Cd(II), and Hg(II) ions due to d^{10} configuration, making developing a new probe is crucial in these cases for their sensing study. For the objective of monitoring heavy metal ions in environmental frameworks optical detection via modifications in UV-visible spectra brought about by heavy metal ions would be very useful. These small-molecule probes may be appropriately incorporated into analytical instruments, optical devices, or advantageous indicators for optical read-outs of heavy metal ions following complexation. This will assist in the quick detection of Pb(II), Cd(II), and Hg(II) ions in the laboratory.

Our experimental outcomes could not be supported well due to lack of literature support on the sensing study of heavy metal ions involving inorganic dithiocarbamate macrocyclic structures by using UV-visible spectral studies. We have selected macrocycles **10-12** for detailed sensing study of toxic heavy metal ions. However, preliminary investigations by UV-visible spectral study reveal that complex **10-12** are showing sensing/binding ability towards soft Hg(II) ions, apparently due to presence of soft sulphur atoms in the metallomacrocyclic framework.

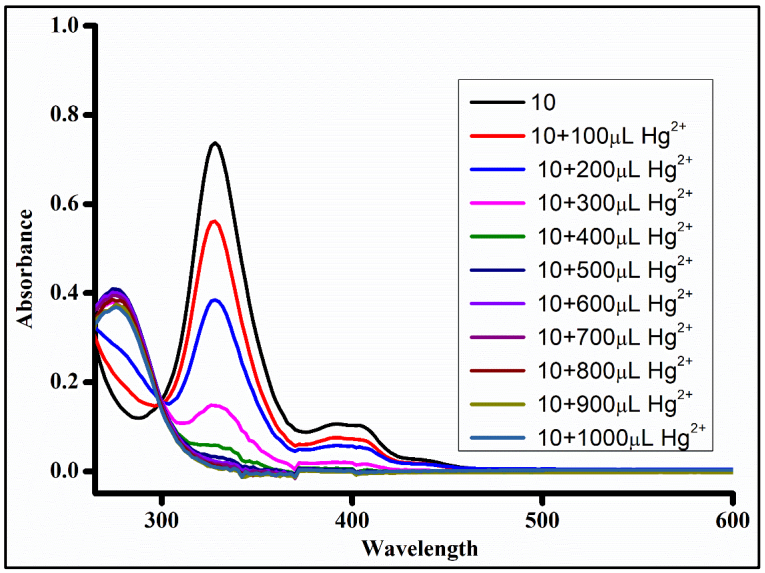

Figure 10. Absorption titration spectra of probe **10** (c, 10 μM) in the presence of various equivalents of Hg(II) ions (0.0−1.0 equiv; 0.4 mM) in DMSO.

The UV-visible titration study (Figure 10) clearly revealed that the peak at 327 nm within the UV-visible spectrum of Ni(II)-dithiocarbamate complex **10** decreased gradually upon the addition of Hg(II), whereas the absorbance intensity at 275 nm gradually increased with one isobestic point[12] determined at 299 nm, indicating that a new product is generated upon binding to Hg(II).

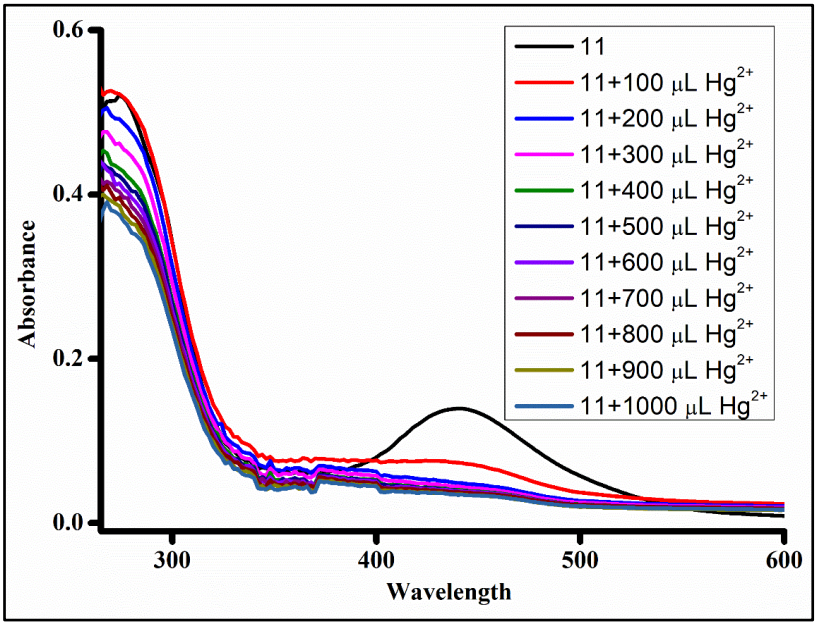

Figure 11. Absorption titration spectra of probe **11** (c, 10 μM) in the presence of various equivalents of Hg(II) ions (0.0−1.0 equiv; 0.4 mM) in DMSO.

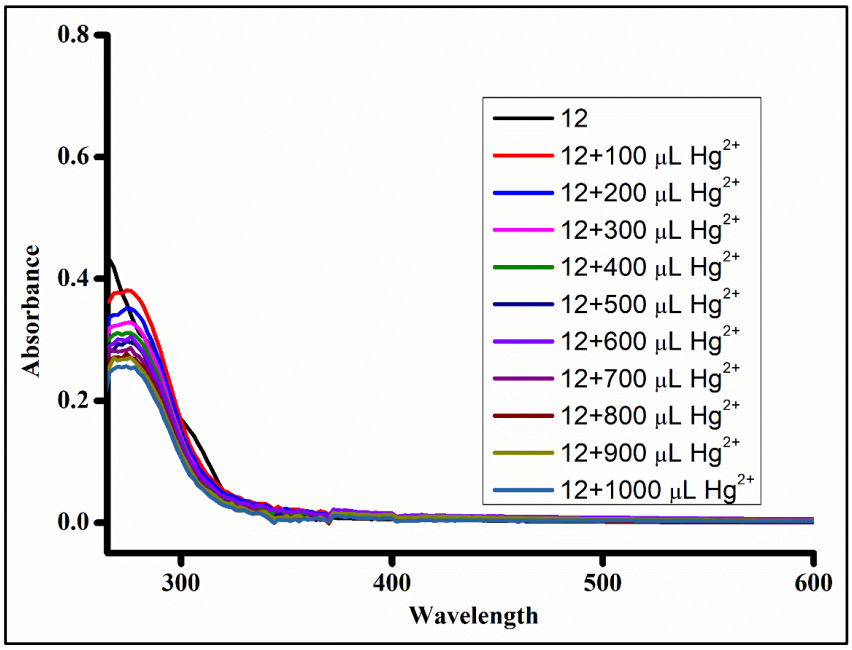

Figure 12. Absorption titration spectra of probe **12** (c, 10 μM) in the presence of various equivalents of Hg(II) ions (0.0−1.0 equiv; 0.4 mM) in DMSO.

The UV-visible titration study clearly revealed that the absorption band at 440 nm within the UV-visible spectrum of Cu(II)-dithiocarbamate complex **11** decreased gradually upon the addition of Hg(II) with a net blue shifting of the absorption band from 273 nm to 268 nm (Figure 11) was observed. In contradiction to this, the addition of Hg(II) indeed inducing a net red shifting of the absorption band from 267 nm to 273 nm in the UV-visible spectrum of Zn(II)-dithiocarbamate complex **12** as shown in Figure 12.

4.5 Conclusions

This study allows us to conclude that a new series of metallomacrocyclic complexes [M(II)$_2$-μ^2-bis-{(κ^2*S*,*S*-S$_2$CN(CH(*S*-CH$_3$)Ph)CH$_2$)$_2$thiophene}]; M = Ni(II) **7**, Cu(II) **8**, Zn(II) **9** and [M(II)$_2$-μ^2-bis-{(κ^2*S*,*S*-S$_2$CN(CH(*R*-CH$_3$)Ph)CH$_2$)$_2$thiophene}]; M = Ni(II) **10**, Cu(II) **11**, Zn(II) **12**, holding thiophene linkers can be conveniently synthesized by using a single pot-multi component reaction protocol. The phase purity and formulation of these were thoroughly verified by microanalysis, relevant spectroscopies, validated by density functional theory calculations. Interestingly, the TG curves of compounds **7, 8, 9** and **11** offered the stable residual mass corresponds to corresponding metal sulphate including some amount of char up to 500 ºC. It is worth noting that the use of soft sulphur donor atoms in the chelating unit of metallomacrocycles **7-12** evidently increase their affinity for Hg(II) ions. A preliminary investigations by UV-visible spectral study suggests complexes **10-12** are able to sense soft Hg(II) ions. Thus such transition metal dithiocarbamate based holding functionalized linkers can be suitably designed as an

analysis tools, optical devices or profitable indicators to assist rapid detections of Hg(II) ions in the laboratory.

4.6 References

[1] Liu, X.; Hamon, J.R. *Coord. Chem. Rev.* **2019**, *389*, 94.

[2] Gregoli ´nski, J.; Slepokura, K.; Kłak, J.; Witwicki, M. *Dalton Trans*. **2022**, *51*, 9735.

[3] Vigato, P.; Tamburini, S.; Bertolo, L. *Coord. Chem. Rev*. **2007**, *251*, 1311.

[4] Chang, F.-F.; Zhang, K.; Huang, W. *Dalton Trans*. **2018**, *48*, 363.

[5] Löffler, M.; Gregoliñski, J.; Korabik, M.; Lis, T.; Lisowski, J. *Dalton Trans.* **2016**, *45*, 15586.

[6] Das, M.; Mukherjee, S.; Koley, B.; Choudhuri, I.; Bhattacharyya, N.; Roy, P.; Samanta, B.C.; Baraif, M.; Maity, T. *New J. Chem*. **2020**, *44*, 18347.

[7] Zhang, J.; Xu, L.; Wong, W.- *Coord. Chem. Rev*. **2018**, *355*, 180.

[8] Janczak, J.; Prochowicz, D.; Lewi ´nski, J.; Fairen-Jimenez, D.; Bereta, T.; Lisowski, J. Eur. J. Chem. **2016**, *22*, 598.

[9] Zhang, X.; Yin, J.; Yoon, J. Chem. Rev. **2014**, *114*, 4918.

[10] Li, Z.-B.; Lin, J.; Sabat, M.; Hyacinth, M.; Pu, L. *J. Org. Chem*. **2007**, *72*, 4905.

[11] Liu, X.; Manzur, C.; Novoa, N.; Celedón, S.; Carrillo, D.; Hamon, J.R. *Coord. Chem. Rev*. **2018**, *357*, 144.

[12] Padnya, P.; Shibaeva, K.; Arsenyev, M.; Baryshnikova, S.; Terenteva, O.; Shiabiev, I.; Khannanov, A.; Boldyrev, A.; Gerasimov, A.; Grishaev, D. *Molecules* **2021**, *26*, 2334.

[13] Che, C.-M.; Huang, J.-S. *Coord. Chem. Rev.* **2003**, *242*, 97.

[14] Shockravi, A.; Javadi, A.; Abouzari-Lotf, E. *RSC Adv.* **2013**, *3*, 6717.

[15] Hajari, S.; Keypour, H.; Rezaei, M.T.; Farida, S.H.M.; Gable, R.W. *J. Mol. Struct*. **2022**, *1251*, 132049.

[16] El-Gammal, O.A.; Mohamed, F.S.; Rezk, G.N.; El-Bindary, A.A. *J. Mol. Liq.* **2021**, *1230*, 129908.

[17] Lee, E.; Lee, S.Y.; Lindoy, L.F.; Lee, S.S. *Coord. Chem. Rev*. **2013**, *257*, 3125.

[18] Tokunaga, H.; Kazama, K.; Tsuboi, M.; Miyasaka, M. *Luminescence*, **2021**, *36*, 1561.

[19] Korupoju, S.R.; Mangayarkarasi, N.; Ameerunisha, S.; Valente, E.J.; Zacharias, P.S. *Dalton Trans.* **2000**, *16*, 2845.

[20] Telfer, S.G.; Sato, T.; Harada, T.; Kuroda, R.; Lefebvre, J.; Leznoff, D.B. *Inorg. Chem.* **2004**, *43*, 6168.

[21] Telfer, S.G.; Kuroda, R. *Coord. Chem. Rev.* **2003**, *242*, 33.

[22] Chinnaraja, E.; Arunachalam, R.; Suresh, E.; Sen, S.K.; Natarajan, R.; Subramanian, P.S. *Inorg. Chem.* **2019**, *58*, 4465.

[23] Chinnaraja, E.; Arunachalam, R.; Samanta, K.; Natarajan, R.; Subramaniana, P.S. *Adv. Synth. Catal.* **2020**, *362*, 1144.

[24] Chinnaraja, E.; Arunachalam, R.; Pillai, R.S.; Peuronen, A.; Rissanen, K.; Subramanian, P.S. *Appl. Organomet. Chem.* **2020**, *34*, e5666.

[25] Castellano, M.; Ruiz-García, R.; Cano, J.; Ferrando-Soria, J.; Pardo, E.; Fortea-Pérez, F.R.; Stiriba, S.-E.; Julve, M.; Lloret, F. *Acc. Chem. Res.* **2015**, *48*, 510.

[26] Ferrando-Soria, J.; Vallejo, J.; Castellano, M.; Martínez-Lillo, J.; Pardo, E.; Cano, J.; Castro, I.; Lloret, F.; Ruiz-García, R.; Julve, M. *Coord. Chem. Rev.* **2017**, *339*, 17.

[27] Žili´c, D.; Rakvin, B.; Mili´c, D.; Paji´c, D.; Đilovi´c, I.; Camettid, M.; Džoli´c, Z. *Dalton Trans*. **2014**, *43*, 11877.

[28] Brown, S.J.; Tao, X.; Wark, T.A.; Stephan, D.W.; Mascharak, P.K. *Inorg. Chem.* **1988**, *27*, 1581.

[29] Sena, N.; Butcher, J.R.; Jasinski, J.P.; Gupta, S.K. *J. Mol. Struct.* **2021**, *1231*, 129955.

[30] Chattopadhyay, T.; Banu, K.S.; Banerjee, A.; Ribas, J.; Majee, A.; Nethaji, M.; Das, D. *J. Mol. Struct*. **2007**, *833*, 13.

[31] Thompson, K.; Mandal, S.K.; Tandon, S.S.; Bridson, J.N.; Park, M.K. *Inorg. Chem.* **1996**, *35*, 3117.

[32] (a)Kadu, R.; Pillai, V.; Amrit, V.; Singh, V. K. *RSC Adv.* **2015**, *5*, 106688. (b) E.-Sonbati, A. Z. *Synth. React. Inorg. Met. -Org. Chem.* **1991**, *21*, 203; (c) Siddiqi, K. S.; Nami, S. A. A. Lutfullah; Chebude, Y. *J. Braz. Chem. Soc.* **2006**, *17*, 107; (d) Bensebaa, F.; Zhou, Y.; Brolo, A. G.; Irish, D. E.; Deslandes, Y.; Kruus, E.; Ellis, T. H. *Spectrochim. Acta*. **1999**, *55A*, 1229.

[33] (a) Cookson, J.; Evans, E. A. L.; Maher, J. P.; Serpell, C. J.; Paul, R. L.; Cowley, A. R.; Drew, M. G. B.; Beer, P. D. *Inorg. Chim. Act.* **2010**, *363*, 1195; (b) Lai, S.-W.; Drew, M. G. B.; Beer, P. D. *J. Organomet. Chem.* **2001**, *637*, 89.

[34] Patel, S. K.; Kolte, K.; Savani, C. J.; Raghavaiah, P.; Dave, D.; Isab, A. A.; Mistry, D.; Suthar, D.; Singh, V. K. *Inorg. Chim. Acta.* **2022**, *543*, 121139.

4.7 Annexures

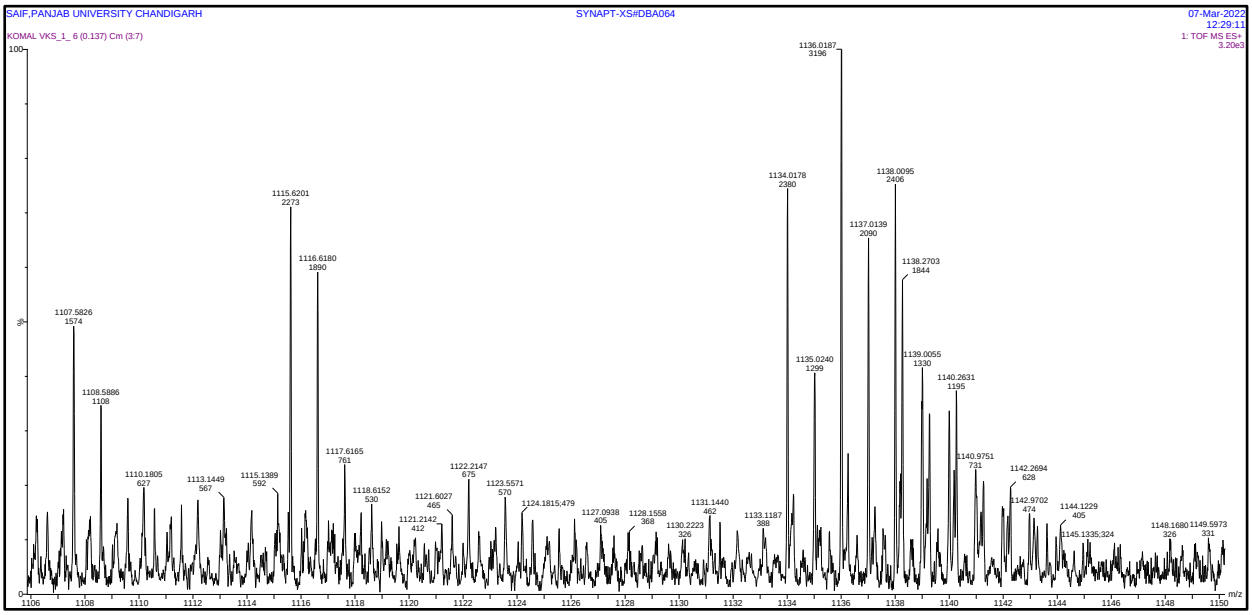

Annexure 1. HRMS spectrum of Complex **7**.

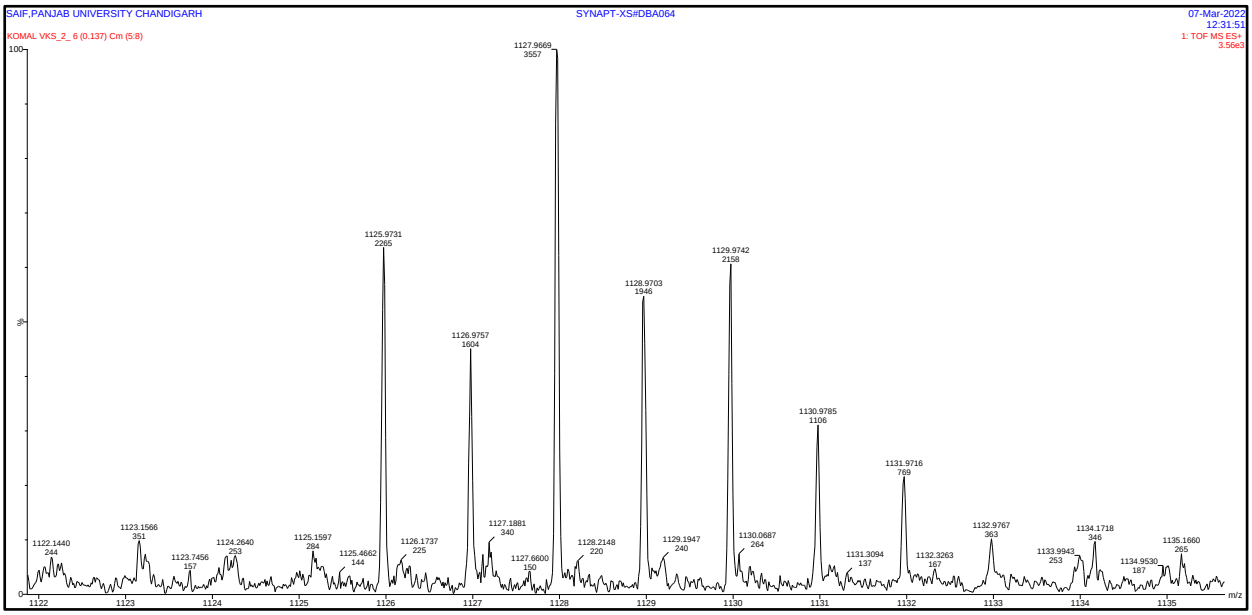

Annexure 2. HRMS spectrum of Complex **8**.

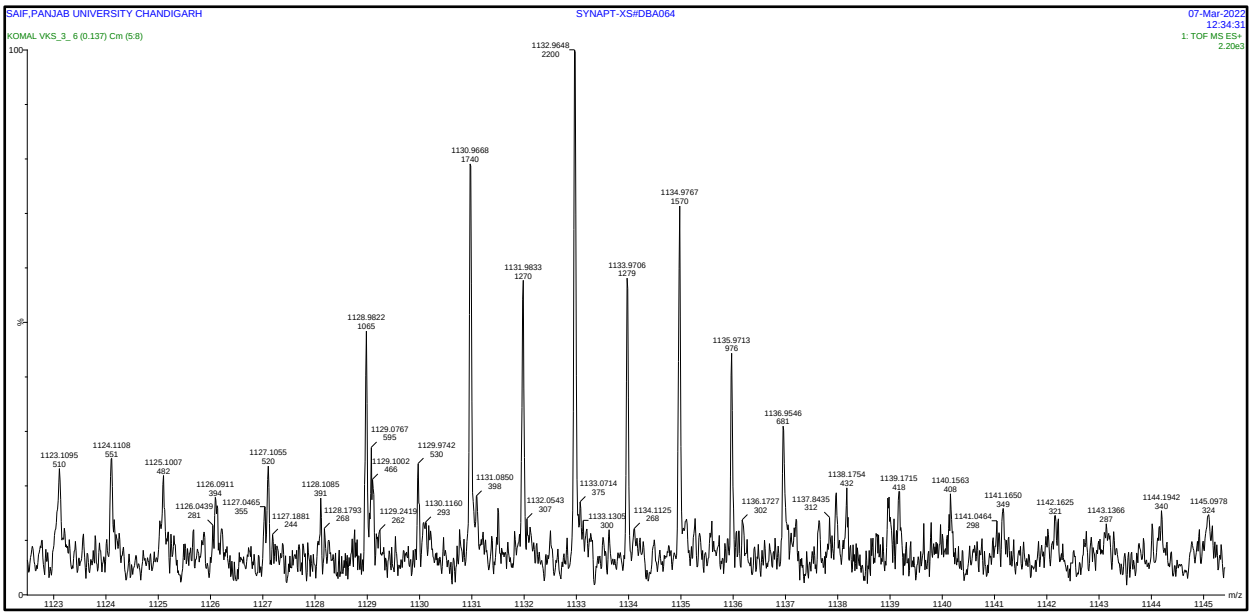

Annexure 3. HRMS spectrum of Complex **9**.

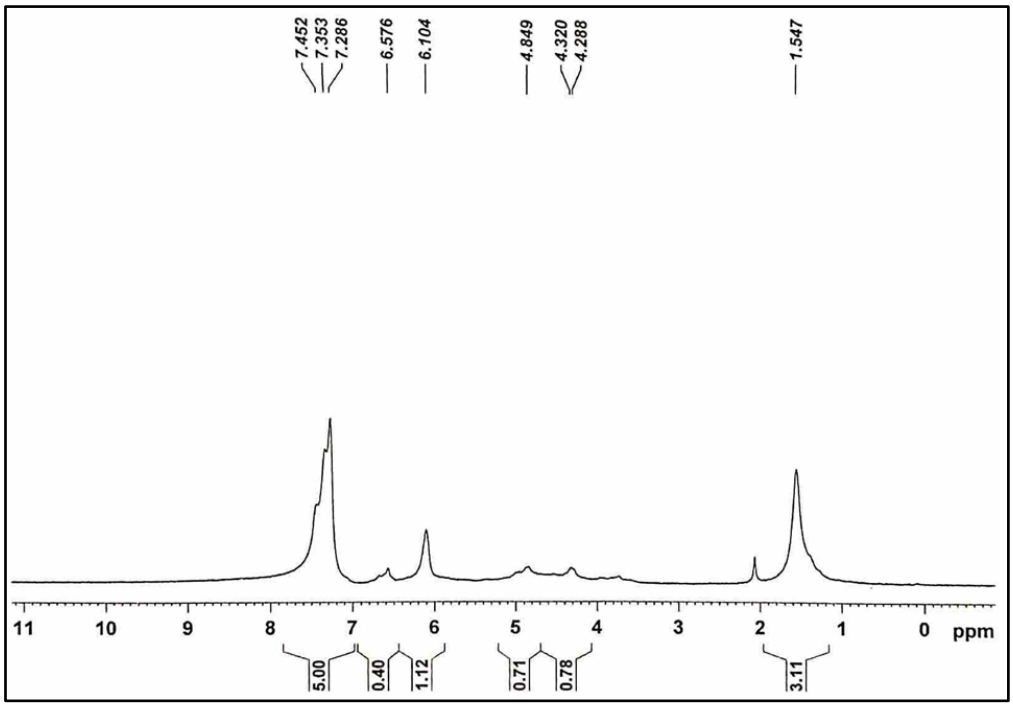

Annexure 4. ^{1}H NMR spectrum of complex **7**.

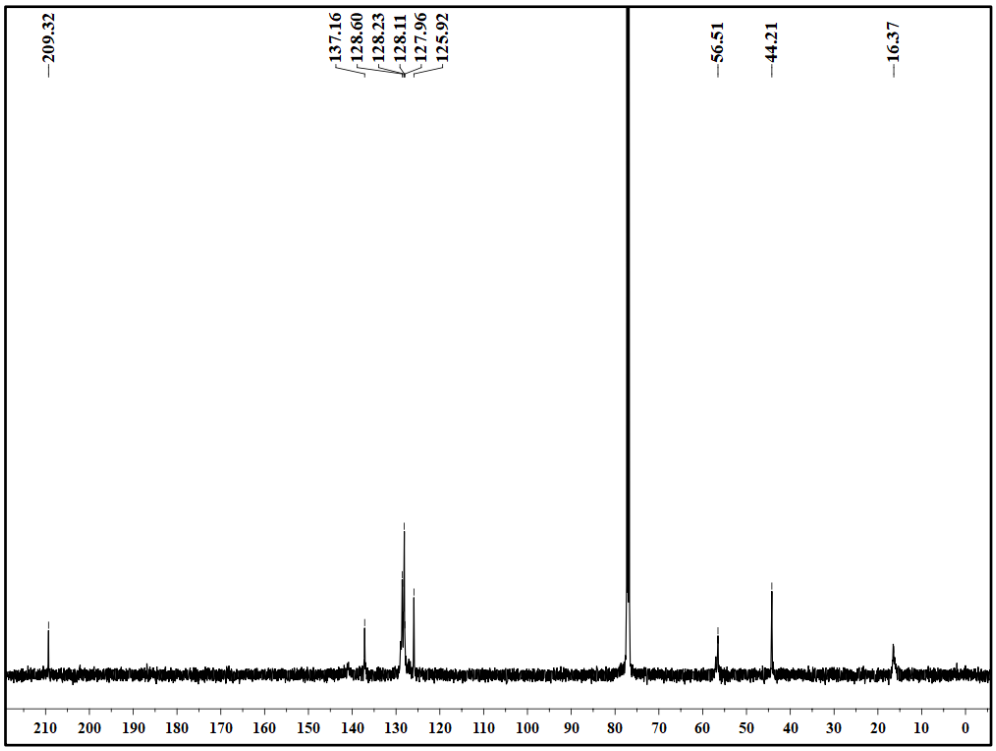

Annexure 5. ^{13}C NMR spectrum of complex **7**.

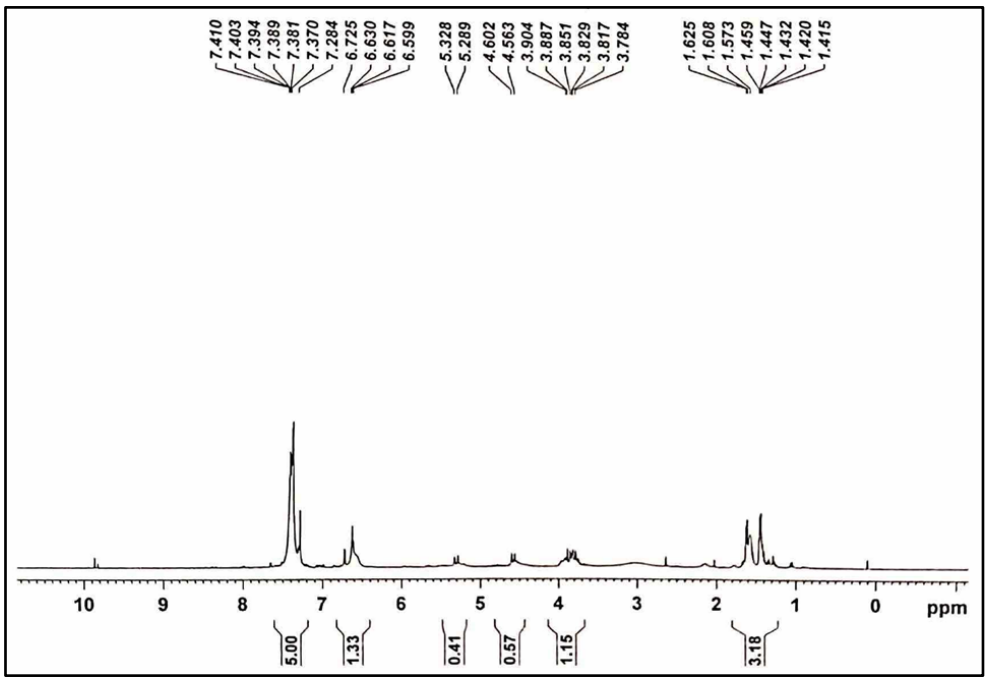

Annexure 6. ^{1}H NMR spectrum of complex **9**.

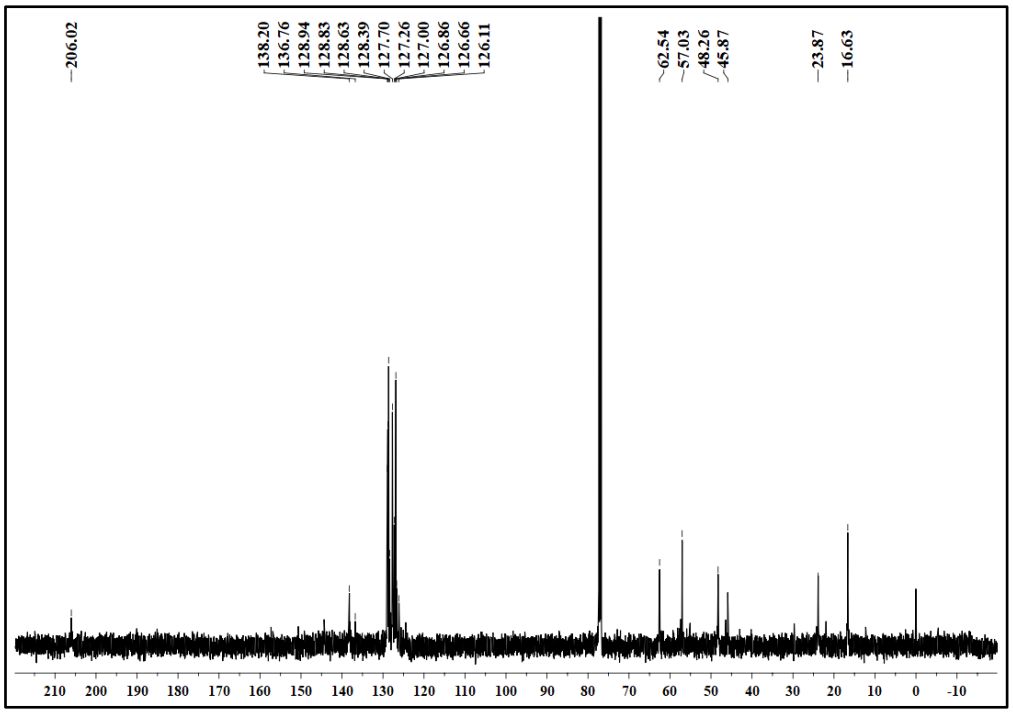

Annexure 7. ^{13}C NMR spectrum of complex **9**.

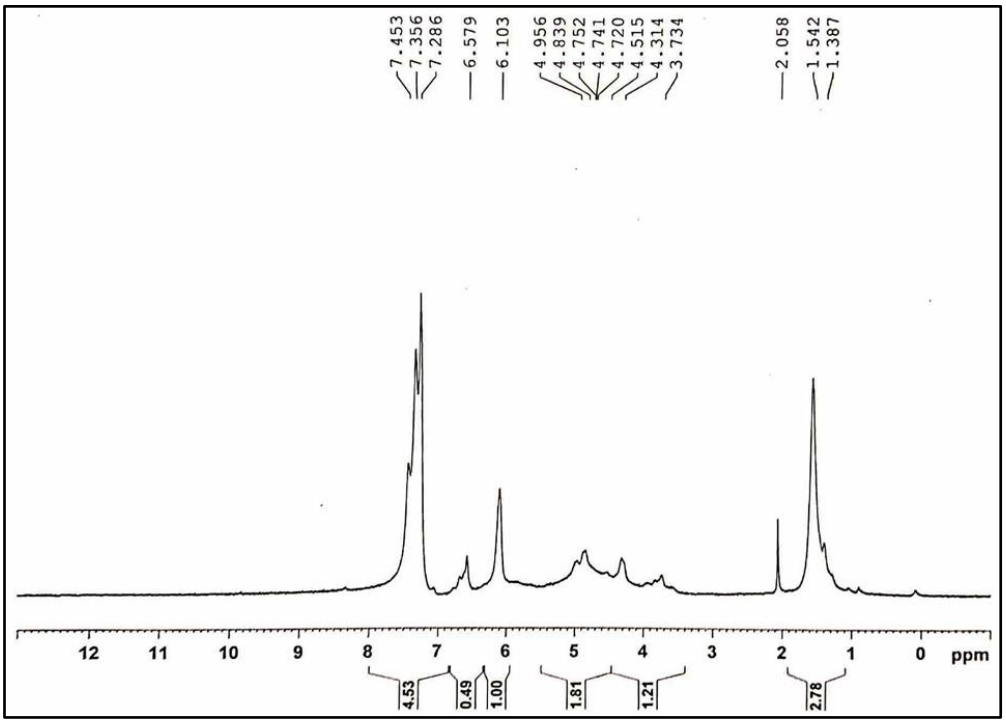

Annexure 8. ^{1}H NMR spectrum of complex **10**.

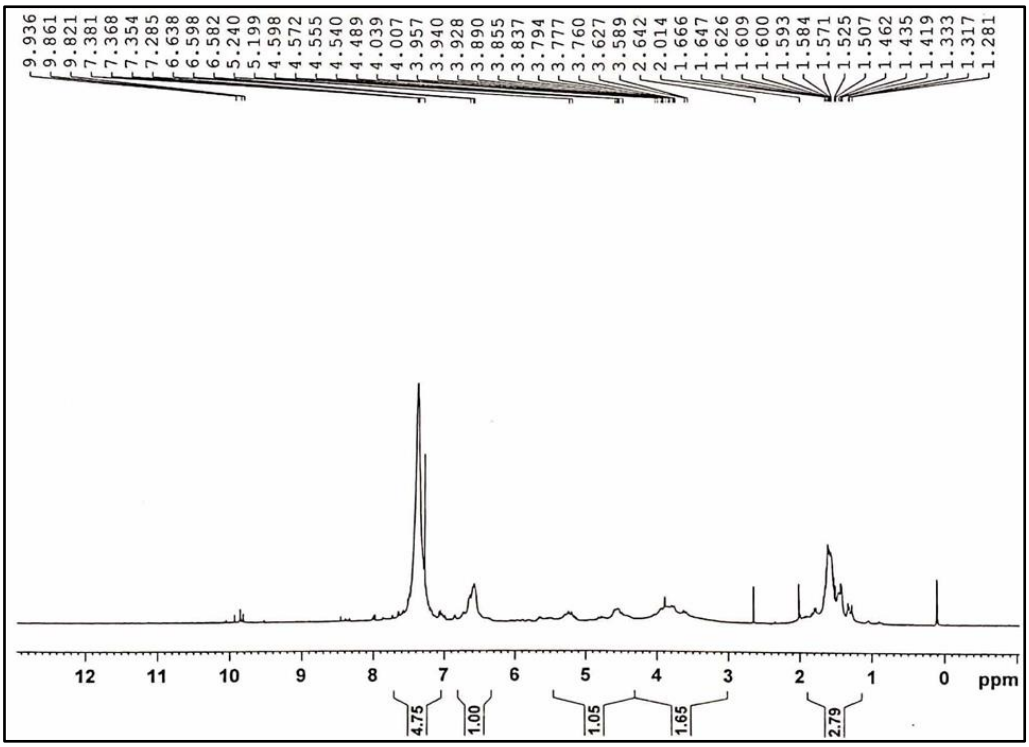

Annexure 9. ^{1}H NMR spectrum of complex **12**.

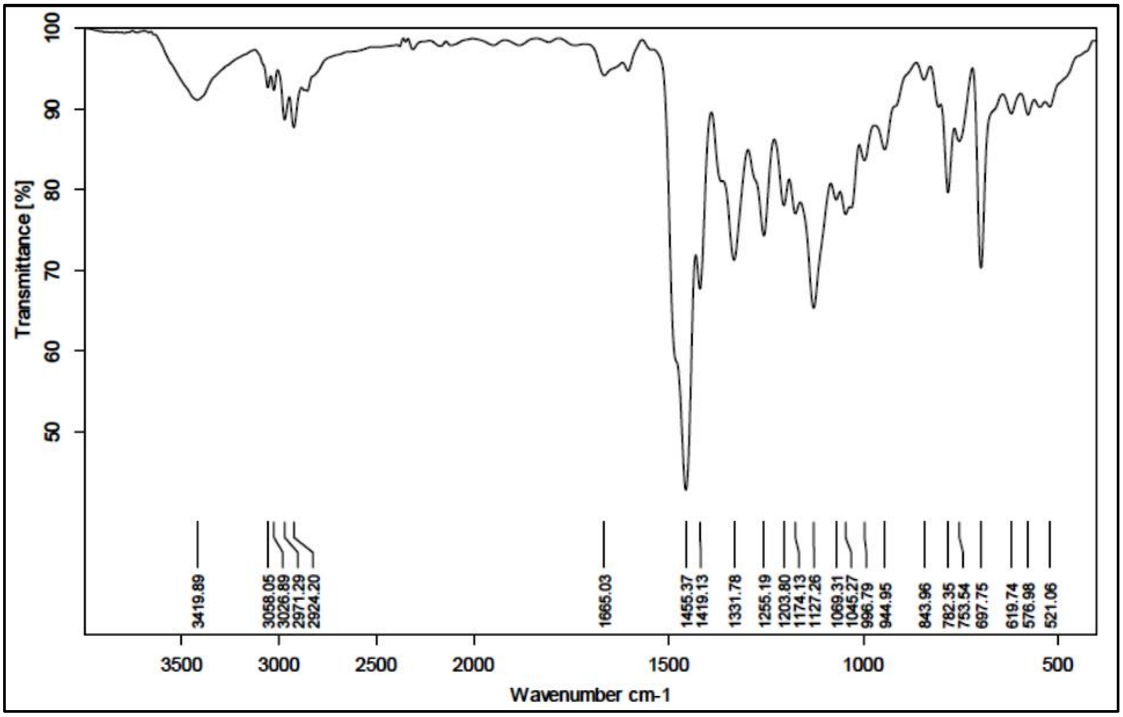

Annexure 10. FTIR spectrum of complex **7.**

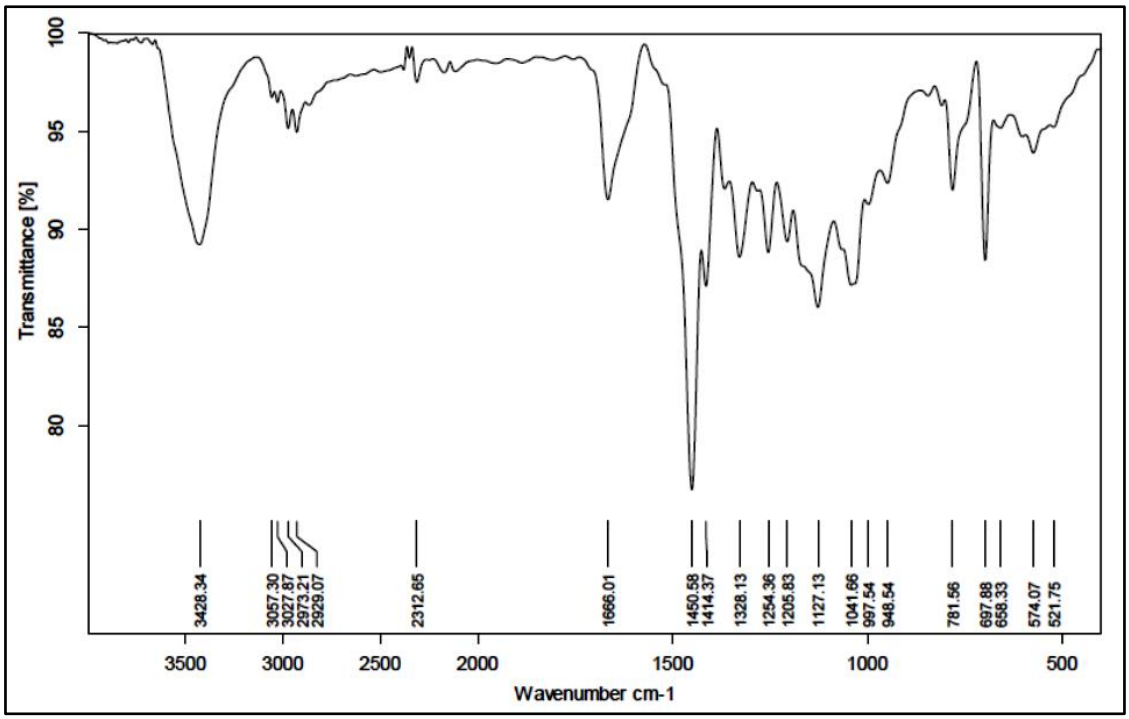

Annexure 11. FTIR spectrum of complex **8.**

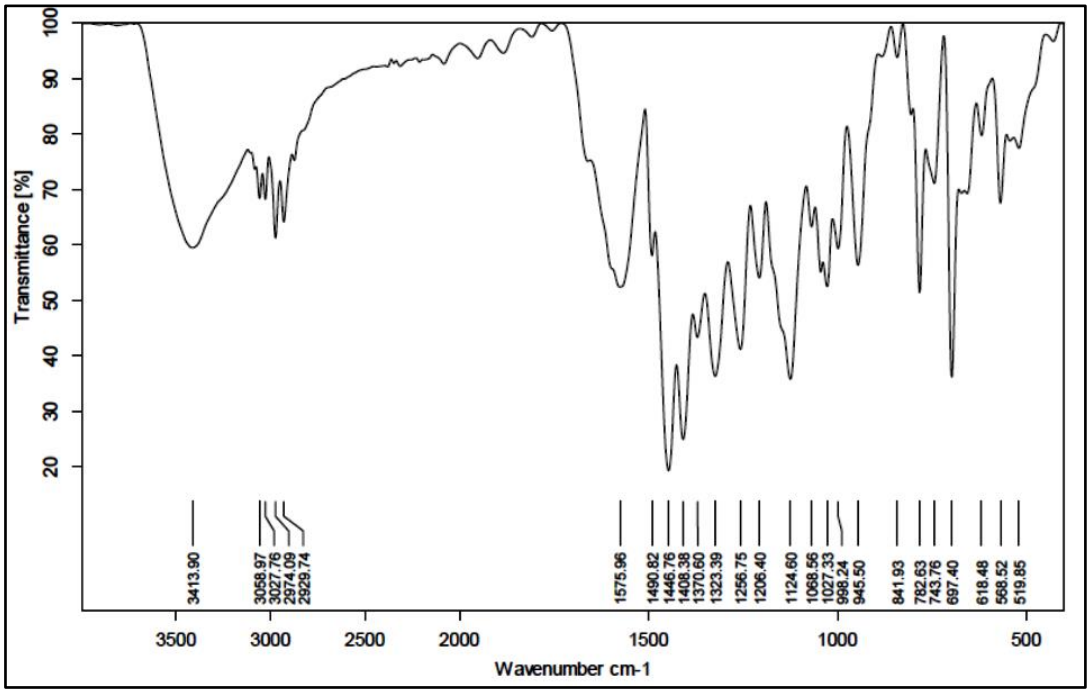

Annexure 12. FTIR spectrum of complex **9.**

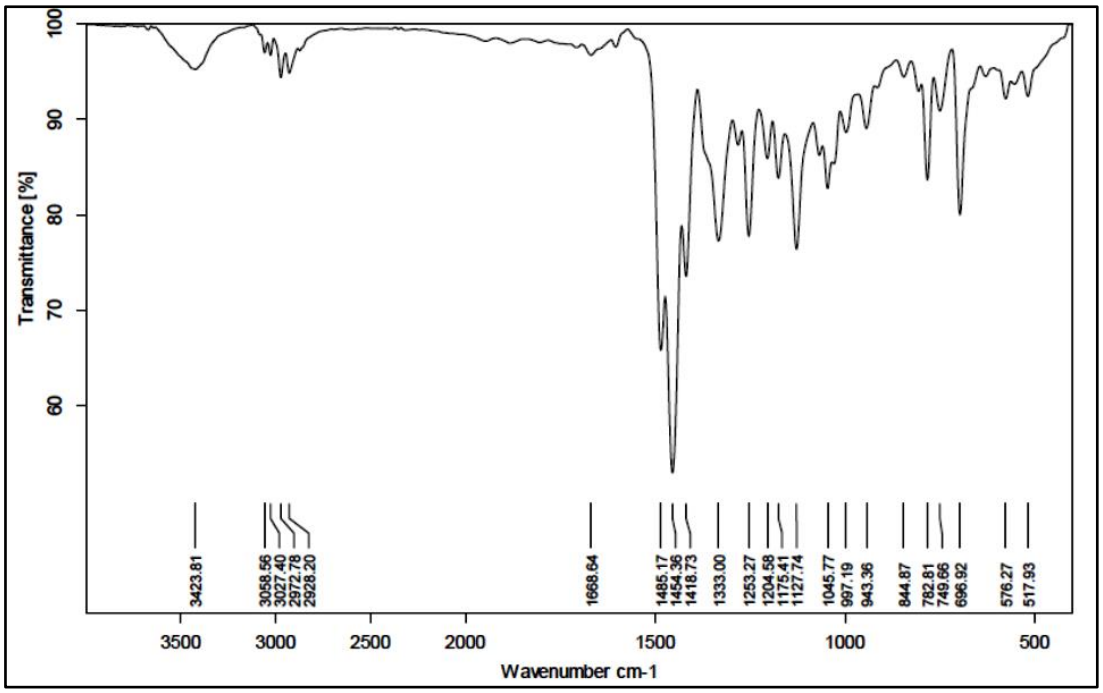

Annexure 13. FTIR spectrum of complex **10.**

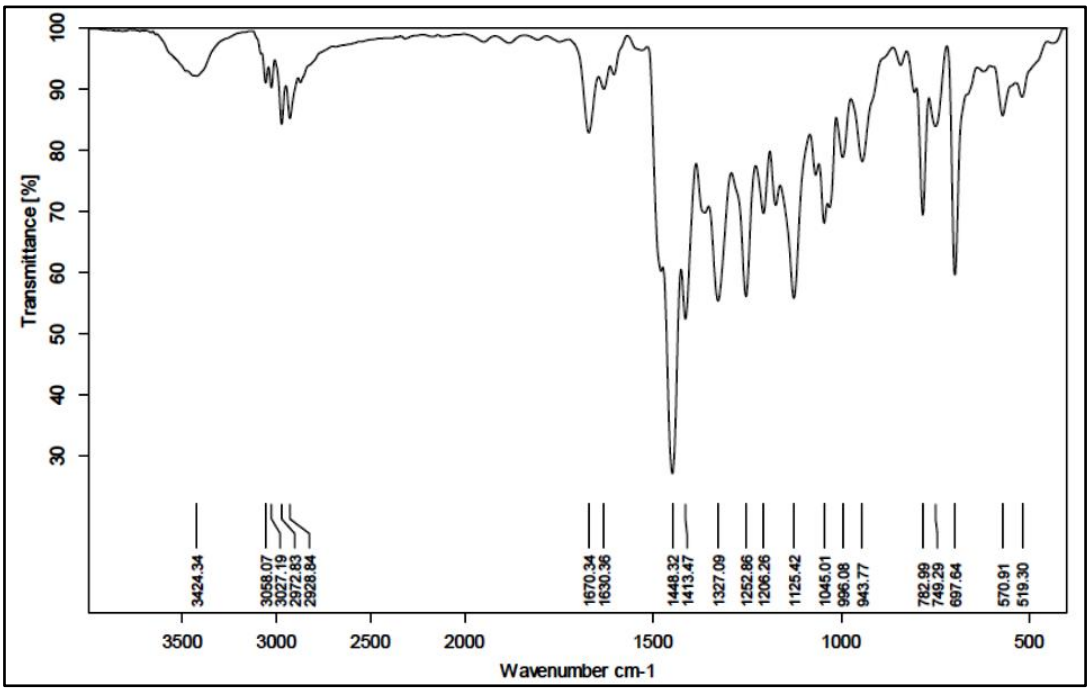

Annexure 14. FTIR spectrum of complex **11.**

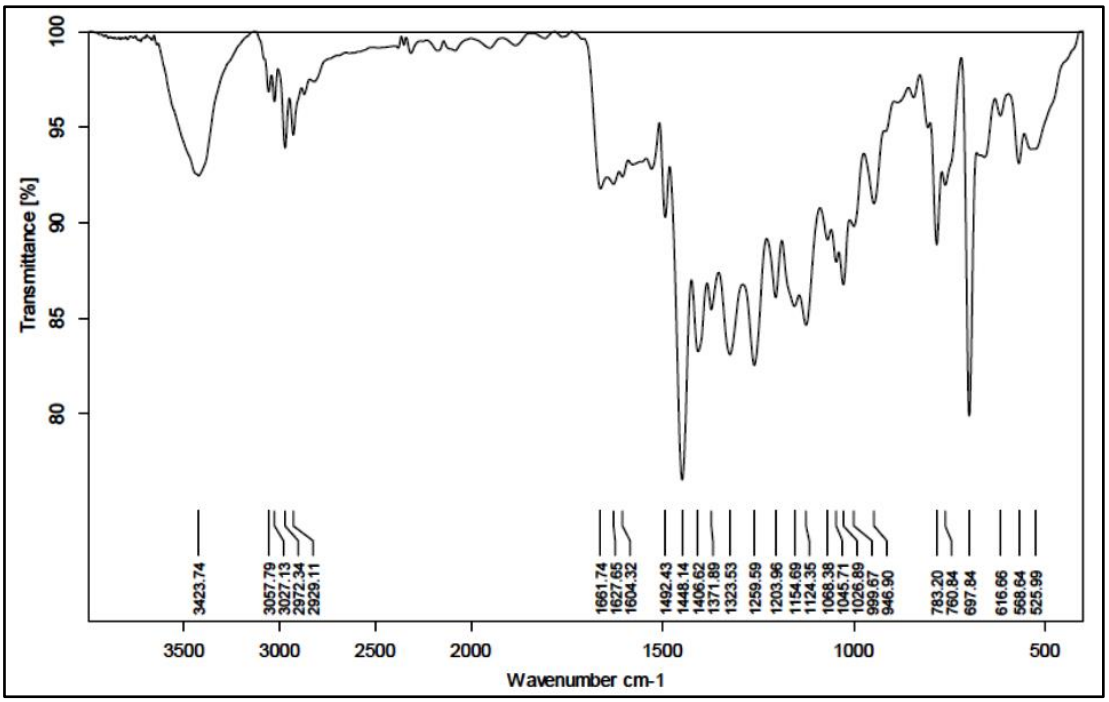

Annexure 15. FTIR spectrum of complex **12.**